

the plasma edge first absorbs laser energy as a result of changes of temperature, ionization degree, and electron density. The pressure distribution in the plasma region is relatively complicated and reaches the order of 10^2 atm. There is a wave hollow 0.2 mm from the target surface, and this is related to the production of a rarefaction wave in the plasma expansion process.

ACKNOWLEDGMENTS

This work was supported by the Trans-Century Training Programme Foundation for the Talents, by the State Education Commission, by the Fok Ying Tung Education Foundation, and by the Nature Science Foundation of Jiansu Province (China).

REFERENCES

1. John F. Ready, *Effects of High-Power Laser Radiation*, Academic Press, New York, 1971, pp. 163.
2. F. Cornolti, A. Giulietti, and D. Giulietti, "Plasma Shape and Shock Structure in a Laser Spark at Low Gas Density," *Opt. Commun.*, Vol. 57, No. 4, 1986, pp. 249.
3. E. Wolf, *Progress in Optics*, North-Holland, Amsterdam, 1985, Vol. XXI, Chap. IV, pp. 199–210.
4. Xiao-Wu Ni, Jian Lu, and An-Zhi He, "Plasma Detection of Field Interaction with Optical Thin Films," *Opt. Commun.*, Vol. 90, No. 2/3, 1992, p. 270.

© 1997 John Wiley & Sons, Inc.
CCC 0895-2477/97

IMPROVED RECOGNITION PERFORMANCE WITH SYNTHETIC CORRELATOR

Farid Ahmed,¹ Abdul A. S. Awwal,² and Mohammad A. Karim³

¹ Electrical Engineering
School of Engineering & Engineering Technology
The Behrend College
Pennsylvania State University
Erie, Pennsylvania 16563

² Computer Science & Engineering Department
Wright State University
Dayton, Ohio 45435

³ Center for Electro-Optics
University of Dayton
Dayton, Ohio 45469

Received 4 November 1996

ABSTRACT: A joint-Fourier-transform (JFT) correlation technique wherein the reference image is synthesized from the point-spread function (PSF) of a preselected filter is investigated. The phase-only filter (POF) and one of its variations are considered to be possible candidates for the synthetic PSF. Filters with optical distortion invariance and higher discrimination can be easily implemented with the use of this technique, resulting in an efficient target recognition system. © 1997 John Wiley & Sons, Inc. *Microwave Opt Technol Lett* 14: 274–278, 1997.

Key words: target recognition; filters; Fourier transform

1. INTRODUCTION

Included among the more significant methods used in optical pattern recognition operations are phase-only-filter (POF) based matched correlation [1], and joint-Fourier-transform

(JFT) correlation [2, 3]. When compared to the classical matched filter [4], a POF results in a sharper correlation peak [1] but it also requires a complex filter fabrication. In comparison, an amplitude-modulated phase-only filter (AMPOF) produces a correlation peak that is sharper than that of the POF [5]. However, it also necessitates accurate alignment of the system. The JFT correlator [2, 3, 6], on the other hand, can be implemented in real time because it requires no complex filter fabrication and generally uses a flexible setup. To ensure sharper correlation peaks in a JFT correlator, however, it becomes necessary to process the joint power spectrum [7–12], but this makes the correlation process somewhat slower.

The motivation to this work is the realization of sharper and more discriminating correlation peaks such as that of a POF or AMPOF in a JFT correlator. The proposed correlator considered herein will thus integrate the best of both the worlds: improved correlation discrimination as well as real-time applications. We also address the possibility of eliminating the postprocessing of binarization and fringe adjustment otherwise necessary in a JFT correlator. This is accomplished by synthesizing the reference image from the point-spread function (PSF) of the corresponding correlation filter. Because the preprocessing is done beforehand, it only incurs a one-time cost. Section 2 discusses the proposed JFT model, and the corresponding simulation results are presented in Section 3. Discussion and conclusions are presented in Section 4.

2. THE SYNTHETIC JFT MODEL

The JFT correlation is a two-step process. In the first step, the joint power spectrum (JPS) of two images placed side by side is obtained by squaring the joint Fourier transform of the input joint image. Then the correlation between the images is extracted by performing an inverse Fourier transform on this JPS. The input joint image $g(x, y)$ is thus given by

$$g(x, y) = s(x, y - d) + t(x, y + d), \quad (1)$$

where $s(x, y - d)$ and $t(x, y + d)$ respectively, represent the object scene and the reference target. The joint Fourier transform of this input results in

$$G(u, v) = S(u, v) \exp(+jvd) + T(u, v) \exp(-jvd), \quad (2)$$

where S and T are the Fourier transforms of the object scene and the reference target, respectively, u and v are independent variables in the frequency domain scaled by a factor $2\pi/\lambda f$, λ is the wavelength of the collimated light, and f is the focal length of the transforming lens. The JPS is given by

$$\begin{aligned} |G(u, v)|^2 &= |S(u, v)|^2 + |T(u, v)|^2 \\ &\quad + S(u, v)T^*(u, v) \exp(+j2vd) \\ &\quad + S^*(u, v)T(u, v) \exp(-j2vd). \end{aligned} \quad (3)$$

In the proposed synthetic JFT model, the reference target is constructed from the PSF of the selected correlation filter. For example, an AMPOF of the reference image can be formulated as follows:

$$H = \frac{De^{j\phi}}{|T| + a}, \quad (4)$$

where D and a are constant parameters. The synthetic reference target is then given by the inverse Fourier transform of H , that is, $\mathcal{F}^{-1}\{H\}$. Note that, because the filter H is Hermitian, the corresponding PSF results in a real image. Now Eq. (3) can be rewritten as

$$|G(u, v)|^2 = |S(u, v)|^2 + |H(u, v)|^2 + S(u, v)H^*(u, v) \exp(+j2vd) + S^*(u, v)H(u, v) \exp(-j2vd). \quad (5)$$

The term $|H(u, v)|^2 = D^2/(|T| + a)^2$ is very small compared to the term $|S(u, v)|^2$. In fact, with proper choice of the parameters D and a , we can find a minimum value for this term. Experimentation with a wide variety of gray images shows that the maximum value of $|H|^2$ is 1.95 for a choice of D and a equal to 1 and 0.1, respectively. In the same simulation the minimum and maximum values of $|S|^2$ are found to be 42 and 5×10^{10} , respectively. Therefore, for all practical purposes, Eq. (5) can be approximated by

$$|G(u, v)|^2 = |S(u, v)|^2 + S(u, v)H^*(u, v) \exp(+j2vd) + S^*(u, v)H(u, v) \exp(-j2vd). \quad (6)$$

The output correlation C is found by subtracting the zero-order term contributed by the input scene (i.e., $|S|^2$) from the JPS and then taking the inverse Fourier transform:

$$C = \mathcal{F}^{-1}\{S(u, v)H^*(u, v) \exp(+j2vd) + S^*(u, v)H(u, v) \exp(-j2vd)\}. \quad (7)$$

Now if the input image s turns out to be the same as the reference target t , this results in deltalike correlation peaks.

A block diagram representation for the simulation procedure is shown in Figure 1. Note that the postprocessing operation uses a computer to subtract out the input-scene-only JPS from the original JPS.

3. SIMULATION AND RESULTS

To validate the performance of the proposed model, two images of a T72 tank at different orientation and one F16 aircraft, as shown in Figure 2, are considered. Each image taken is of 32×32 size, and the joint image is of size 256×256 . For the simulation results of Tables 1 and 2, the T72 serves as the reference image. The synthetic reference, that is, $t(x, y)$, is then derived from the PSF of the filter, described by Eq. (4) with the use of the 256×256 2D FFT. Three cases are considered in the simulation: (a) an object scene containing an F16 as the input image, which is a nontarget; (b) an object scene containing a T72 tank as the input image, which is a target; and (c) an object scene containing both an F16 (nontarget) and a T72 (target).

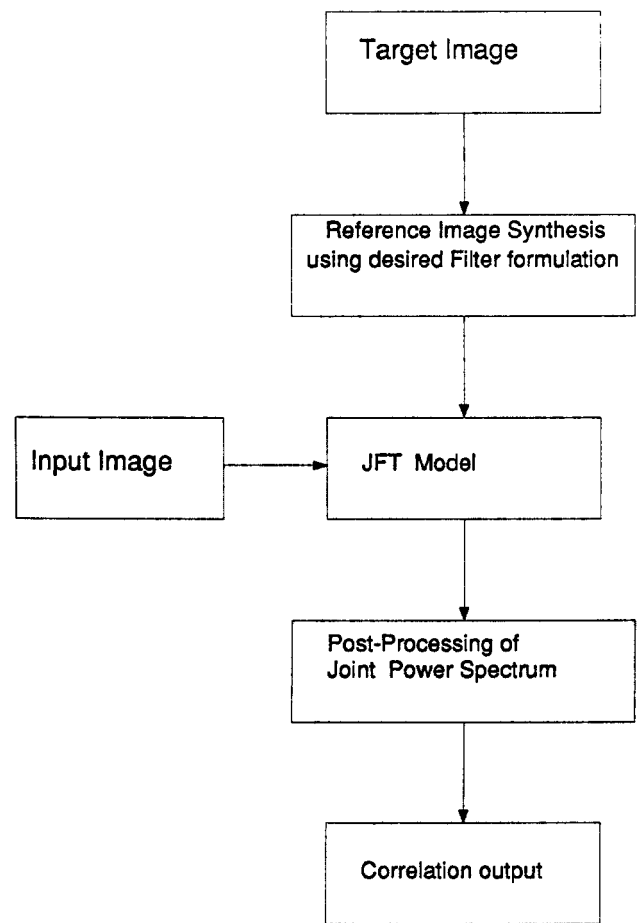


Figure 1 Block diagram of the simulation procedure



Figure 2 The images: (a) T72 and (b) F16

Performance criteria considered are normalized peak (NP), peak-to-average correlation energy ratio (PACE), peak-to-side-lobe ratio (PSR), correlation width (CW), and discrimination ratio (DR). NP is defined as the peak value of a ratio of the total correlation values, which is scaled to a factor of

TABLE 1 Single-Object Correlation Performance

Performance Criterion	Classical JFT		Binarized JFT		SJFT (POF)		SJFT (AMPOF)	
	Target	NT	Target	NT	Target	NT	Target	NT
NP	0.135	0.118	1.46	0.1521	1.78	0.52	246.2	.082
PACE	61.1	54	17354	231	6560	892	65536	119.5
PSR	0.0053	0.0057	1.87	0.0127	0.112	0.0182	$3.0e + 07$	0.0045
CW	(21,21)	(25,25)	(1,1)	(4,4)	(1,1)	(7,7)	(1,1)	(10,10)
DR	1.4		75		7.4		548	

NT—nontarget.
SJFT—synthetic JFT.

TABLE 2 Multiple-Object Correlation Performance

Performance Criterion	Classical JFT	Binarized JFT	SJFT (POF)	SJFT (AMPOF)
NP	0.079	1.0086	1.05	1.11
PACE	37.73	10871	4688	17686
PSR	0.0051	1.117	0.112	1.77
DR	3.08	18.53	18.4	202.7
CW	(21,21)	(1,1)	(1,1)	(1,1)

SJFT—synthetic JFT

255 [5]. This metric is useful for measuring the relative correlation peak value. PACE is the ratio of the correlation peak intensity to the average correlation plane energy [14]. This measures the intensity of energy concentration in the correlation peak in terms of the average energy in a pixel. PSR is defined as the ratio of the autocorrelation peak intensity to the correlation power in the side lobe [14]. The side lobe here is taken as the correlation area where the intensity is less than 50% of the correlation peak. This is a relative measure of the autocorrelation peak sharpness with respect to the side-lobe width and intensity. CW is the width of the correlation term at half its peak value [13]. DR, on the other hand, is defined as the square of the ratio of the autocorrelation peak to the cross-correlation peak [14]. This is often the most useful metric where consideration of discrimination between target and nontarget is of prime importance.

First, the simulation is performed with a single object present in the input scene. Figure 3 shows the corresponding autocorrelation (with object scene having the target) and cross correlation (with object scene having a nontarget) outputs with the use of simulation models of (a) a classical JFT correlator, and (b) the proposed JFT correlator based on the PSF of the POF of the original reference. Similarly, Figure 4 shows the outputs with the use of (a) a binarized JFT correlator, and (b) the proposed JFT correlator based on the PSF of AMPOF of the original reference. The classical peaks are seen to have, as expected, lower normalized power, wider

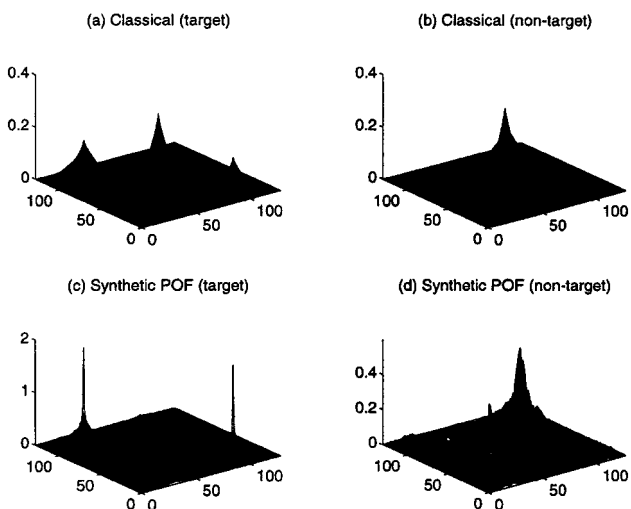


Figure 3 Single-object correlation: (a) classical JFT with object scene including only the target, (b) classical JFT with object scene including only the nontarget, (c) synthetic POF-based JFT with object scene including only the target, (d) synthetic POF-based JFT with object scene including only the nontarget

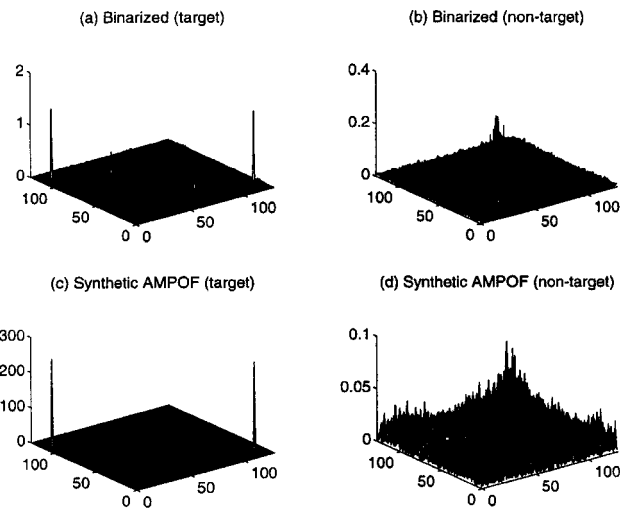


Figure 4 Single-object correlation: (a) binarized JFT with object scene including only the target, (b) binarized JFT with object scene including only the nontarget, (c) synthetic AMPOF-based JFT with object scene including only the target, (d) synthetic AMPOF-based JFT with object scene including only the nontarget

correlation width, and lower discrimination capability. The performance criteria for these correlators are enumerated in Table 1. Note that in the case of the binarized JFT, the JPS is binarized with the use of median thresholding [7]. The most meaningful result obtained from the proposed model with AMPOF PSF is its discrimination capability, which is improved sevenfold over the binarized JFT. Comparing the other figures of merit, it is seen that for the synthetic JFT with AMPOF PSF, NP improves 168 fold, and PACE and PSR are increased by factors of 3.77 and 1.6×10^7 , respectively. The synthetic JFT with the POF PSF yielded better results than the binarized one in terms of the normalized peak, whereas its PACE and PSR values are lower than those of the binarized JFT.

Next, the model was tested with the use of multiobject input scenes. Accordingly, we here consider an object scene that contains one target (i.e., T72) and one nontarget (i.e., F16). Figures 5–8 illustrate the correlation output resulting from the four correlator models: classical, binarized, synthetic POF-based JFT and synthetic AMPOF-based JFT correlators. Autocorrelation peaks are on the upper left and lower right, whereas the cross-correlation peaks are on the

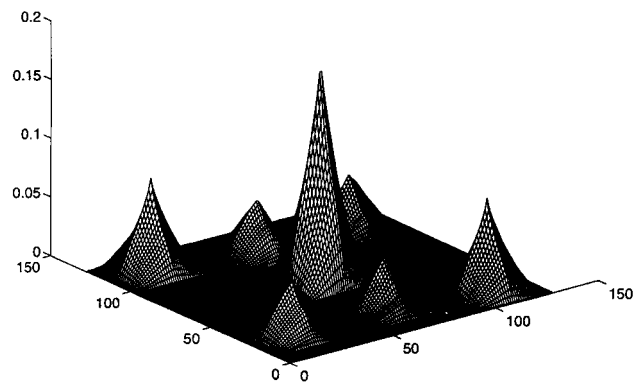


Figure 5 Multiple-object correlation with the use of a classical JFT correlator

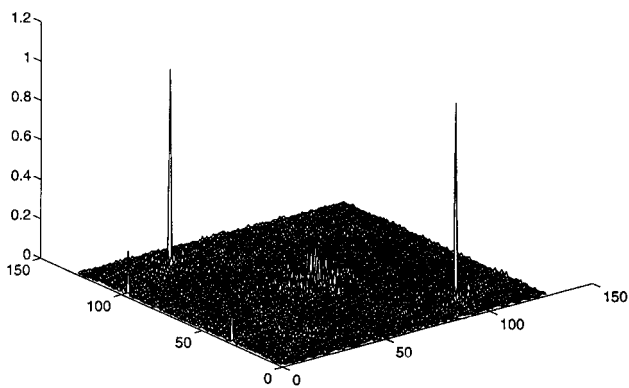


Figure 6 Multiple-object correlation with the use of a binarized JFT correlator

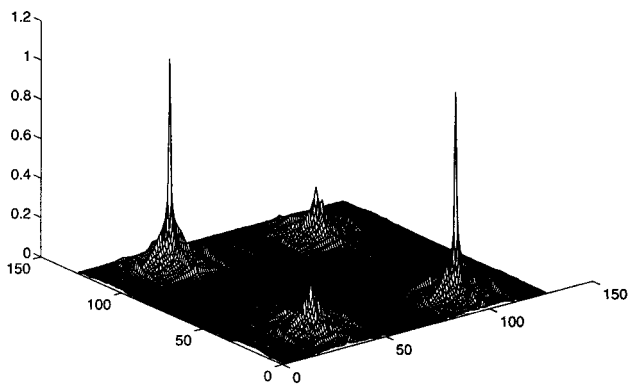


Figure 7 Multiple-object correlation in a synthetic POF-based JFT correlator

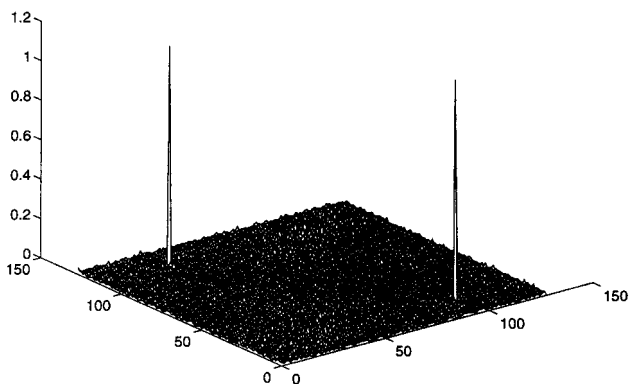


Figure 8 Multiple-object correlation in a synthetic AMPOF-based JFT correlator

upper right and lower left. Table 2 enumerates the performance comparisons among these schemes. Here also, the DR for the AMPOF-based synthetic JFT model has improved 10.9 times over binarized JFT. The NP, PACE, and PSR are also found to be the best in this model. As in the case of the single object, the POF-based synthetic JFT model performs well in terms of the NP. The DR value is comparable to that of the binarized JFT while considering PACE, and PSR, the POF-based synthetic JFT model, does not exhibit any distinct advantage. Among all four correlators, the synthetic JFT model based on the AMPOF PSF demonstrates the best correlation performance.

To validate the above-mentioned results still further, we have experimented with a variety of images. For each of these simulations the correlation performance was qualitatively found to be the same as that mentioned in Tables 1 and 2. For the sake of clarity, we here furnish the average correlation performance of six simulation runs for the multiobject case. These six different cases are obtained from the three images (the combination of one image as a reference and one of two others in the input scene along with the reference). Table 3 summarizes the mean and standard deviation of the performance criterions. Note particularly that the same qualitative correlation performances are obtained with the various correlator models considered.

Next, an interesting variation of the synthetic JFT model based on AMPOF PSF is investigated. In the case of the multiple object scene, *zero thresholding* of the modified power spectrum is carried out. Let the dc subtracted power spectrum be P . The thresholded spectrum (P_t) is then given by

$$P_t = \begin{cases} +1, & \text{if } P > 0, \\ -1, & \text{otherwise.} \end{cases} \quad (8)$$

This means that the power spectrum is now binarized to +1 or -1, depending upon whether the original power spectrum values are larger or smaller than 0. Note that the threshold value of 0 is known beforehand. It is therefore easy to implement, thus reducing the computational burden of median calculation otherwise necessary in the binarized JFT used in Reference 7. Figure 9 shows the corresponding correlation output. The NP is now increased by a factor of 1.77. The PACE and PSR values are increased to 33,263 (1.88 times) and 3.87 (2.19 times), respectively. The discrimination ratio, however, is reduced to 68, but the value still remains higher than that of binarized JFT, which has a value of 18.53.

4. CONCLUSION

In this work we have explored a novel method for target recognition with the use of the synthesized PSF of two correlation filters in a JFT architecture. Because the reference image synthesis is accomplished off-line, it does not slow down the real-time recognition applications. The synthetic

TABLE 3 Average Correlation Performance for Multiple-Object JFT

Performance Criterion	Classical JFT		Binarized JFT		SJFT (POF)		SJFT (AMPOF)	
	Mean	Std	Mean	Std	Mean	Std	Mean	Std
NP	0.069	0.0068	0.8	0.14	0.82	0.16	0.98	0.17
PACE	28.2	5	7410	1540	4112	1015	12514	2530
PSR	0.0052	0.0001	0.86	0.17	0.103	0.01	1.41	0.24
DR	2.1	0.68	20.2	3.1	14.2	4.3	124	23

Std—standard deviation.

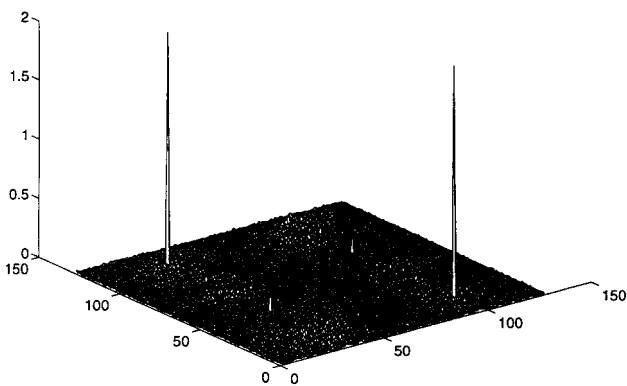


Figure 9 Zero-thresholded correlation output for the AMPOF-based JFT model

JFT based on AMPOF PSF yields better performance in terms of the normalized peak power, peak-to-side-lobe ratio, discrimination ratio, and correlation width. Median computation and thresholding of the binarized JFT are sequential in nature, and therefore time consuming. The proposed JFT model drastically reduces the amount of time because it involves neither any median-based thresholding nor postmultiplication of the fringe pattern. Although the results mentioned here are scene specific, the trend is similar for a wide range of images that we have studied. This scheme can easily be applied to any optimal pattern recognition filter.

REFERENCES

1. P. D. Gianino and J. L. Horner, "Phase-Only Matched Filtering," *Appl. Opt.*, Vol. 23, 1984, pp. 812–816.
2. F. T. S. Yu and J. E. Ludman, "Microcomputer Based Programmable Joint Transform Correlator for Automatic Pattern Recognition and Identification," *Opt. Lett.*, Vol. 11, 1986, pp. 395–397.
3. B. Javidi and C. Kuo, "Joint Transform Image Correlation Using a Binary Spatial Light Modulator at the Fourier Plane," *Appl. Opt.*, Vol. 27, 1988, pp. 663–665.
4. A. VanderLugt, "Signal Detection by Complex Spatial Filtering," *IEEE Trans. Inf. Theory*, Vol. IT-10, 1964, pp. 139–145.
5. A. A. S. Awwal, M. A. Karim, and S. R. Jahan, "Improved Correlation Discrimination Using an Amplitude-Modulated Phase-Only Filter for Optimum Recognition," *Appl. Opt.*, Vol. 29, 1990, pp. 233–236.
6. O. Perez and M. A. Karim, "An Efficient Implementation of Joint Fourier Transform Correlation Using a Modified LCTV," *Microwave Opt. Technol. Lett.*, Vol. 2, 1989, pp. 193–196.
7. B. Javidi, "Nonlinear Joint Power Spectrum Based Optical Correlation," *Appl. Opt.*, Vol. 28, 1989, pp. 2358–2367.
8. S. K. Rogers, J. D. Cline, and M. Kabrisky, "New Binarization Techniques for Joint Transform Correlation," *Opt. Eng.*, Vol. 29, 1990, pp. 1018–1093.
9. M. S. Alam, A. A. S. Awwal, and M. A. Karim, "Improved Correlation Discrimination Using Joint Fourier Transform Optical Correlator," *Microwave Opt. Technol. Lett.*, Vol. 4, 1991, pp. 103–106.
10. M. S. Alam and M. A. Karim, "Fringe-Adjusted Joint Transform Correlator," *Appl. Opt.*, Vol. 32, 1993, pp. 4351–4356.
11. S. Vallmitjana, A. Carnicer, E. Martin-Badosa, and I. Juvells, "Nonlinear Filtering in Object and Fourier Space in a Joint Transform Optical Correlator: Comparison and Experimental Realization," *Appl. Opt.*, Vol. 34, No. 20, 1995, pp. 3942–3949.
12. J. Wang and B. Javidi, "Multiobject Detection Using the Binary Joint Transform Correlator with Different Types of Thresholding Methods," *Opt. Eng.*, Vol. 33, 1994, pp. 1793–1805.
13. B. Javidi, and S. F. Odeh, "Multiple Object Identification by

Bipolar Joint Transform Correlation," *Opt. Eng.*, Vol. 27, 1988, pp. 295–300.

14. B. V. K. Vijaya Kumar and L. Hassebrook, "Performance Measures for Correlation Filters," *Appl. Opt.*, Vol. 29, 1990, pp. 2997–3006.

© 1997 John Wiley & Sons, Inc.
CCC 0895-2477/97

IMPROVED FORM OF BACKFIRE BIFILAR HELIX CONICAL BEAM ANTENNA

K. M. Keen,¹ D. Smith,² and B. S. Lee³

¹ Keen Associates

Ifold, West Sussex RH14 OTA, United Kingdom

² Department of Electrical, Electronic Engineering and Physics

University of Northumbria at Newcastle

Newcastle upon Tyne NE1 8ST, United Kingdom

³ Matra Marconi Space UK Ltd.

First Avenue

Poynton, Stockport, Cheshire SK12 1NE, United Kingdom

Received 5 November 1996

ABSTRACT: The nonresonant-length backfire bifilar helix is often used as a vehicle satcom antenna, as it has a circularly polarized conical beam with azimuthal symmetry. Some antenna configurations, however, exhibit poor back-lobe levels. It is shown that radiation patterns can be significantly improved by correct termination of the helix. © 1997 John Wiley & Sons, Inc. *Microwave Opt Technol Lett* 14: 278–280, 1997.

Key words: antennas; helical antennas; bifilar helix antenna

1. INTRODUCTION

Backfire bifilar helix antennas with nonresonant-length helical wires and small diameters have the ability to form conical-shaped beams that are circularly polarized. This was first demonstrated by Patton [1], and for this reason the antenna is sometimes referred to as the Patton coil [2]. With the use of the coordinate system shown in Figure 1, this type of antenna exhibits a conical beam with a peak at some value of θ between 0° and 90° , and with symmetry about the Z axis, when the two helical conductors are excited in antiphase at the top T and with the helical windings shorted together at the bottom, at O . The elevation angle of the beam peak depends on the helix diameter and pitch angle, and the beamwidth of the conical beam depends on the overall length (and therefore the number of turns) of the helix. In general, more turns give narrower beamwidths. The sense of the helical windings determines whether the antenna operates in RHCP or LHCP.

Because of the conical beam shape, this type of antenna is often used for satcom terminals on vehicles. Terminal antenna dimensions are typically 3–5 wavelengths in length and 0.05–0.1 wavelength in diameter. Antennas with mechanically variable helix dimensions have been demonstrated. With these, the beam elevation angle can be manually adjusted for a wide range of satellite elevation angles [3].

One disadvantage of the backfire bifilar helix antenna is that with some configurations, the radiation pattern back-lobe levels are high. Kilgus [4] has shown that this problem can be overcome with a more complex quadrifilar form of backfire